JACS Au
AN OPEN ACCESS JOURNAL OF THE AMERICAN CHEMICAL SOCIETY

pubs.acs.org/jacsau

Article

Human Serum Albumin–Oligothiophene Bioconjugate: A Phototheranostic Platform for Localized Killing of Cancer Cells by Precise Light Activation

Andrea Cantelli, Marco Malferrari, Alice Soldà, Giorgia Simonetti, Sonny Forni, Edoardo Toscanella, Edoardo J. Mattioli, Francesco Zerbetto, Alberto Zanelli, Matteo Di Giosia, Mattia Zangoli, Giovanna Barbarella, Stefania Rapino,* Francesca Di Maria,* and Matteo Calvaresi*

Cite This: *JACS Au* 2021, 1, 925–935

Read Online

ACCESS | Metrics & More | Article Recommendations | Supporting Information

ABSTRACT: The electronic, optical, and redox properties of thiophene-based materials have made them pivotal in nanoscience and nanotechnology. However, the exploitation of oligothiophenes in photodynamic therapy is hindered by their intrinsic hydrophobicity that lowers their biocompatibility and availability in water environments. Here, we developed human serum albumin (HSA)–oligothiophene bioconjugates that afford the use of insoluble oligothiophenes in physiological environments. UV–vis and electrophoresis proved the conjugation of the oligothiophene sensitizers to the protein. The bioconjugate is water-soluble and biocompatible, does not have any "dark toxicity", and preserves HSA in the physiological monomeric form, as confirmed by dynamic light scattering and circular dichroism measurements. In contrast, upon irradiation with ultralow light doses, the bioconjugate efficiently produces reactive oxygen species (ROS) and leads to the complete eradication of cancer cells. Real-time monitoring of the photokilling activity of the HSA–oligothiophene bioconjugate shows that living cells "explode" upon irradiation. Photodependent and dose-dependent apoptosis is one of the primary mechanisms of cell death activated by bioconjugate irradiation. The bioconjugate is a novel theranostic platform able to generate ROS intracellularly and provide imaging through the fluorescence of the oligothiophene. It is also a real-time self-reporting system able to monitor the apoptotic process. The induced phototoxicity is strongly confined to the irradiated region, showing localized killing of cancer cells by precise light activation of the bioconjugate.

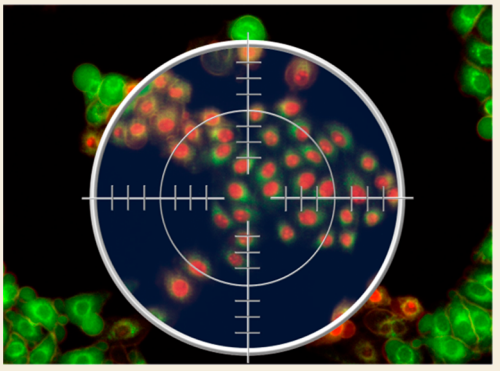

KEYWORDS: *oligothiophenes, human serum albumin, bioconjugate, phototheranostics, reactive oxygen species, photostimulated apoptosis, photodynamic therapy*

INTRODUCTION

Multifunctionality, chemical robustness, and versatility of chemical systems are some of the fundamental requirements in nanoscience and nanotechnology. Oligothiophenes fit the bill and have been used for a number of high-tech applications, including organic light-emitting diode (OLED), organic field-effect transistor (OFET), light-emitting transistors (LET), lasers, biosensors, chemosensors, and electrochromic devices.[1−6] The photophysics of oligothiophenes is characterized by high absorbance, bright fluorescence, and high chemical and optical stability. Their fluorescence can be modulated by exploiting any of the numerous and well-established synthetic protocols that can change the number of thiophene rings and the nature of side-chains attached to them.[7] Indeed, thiophene oligomers are intensely exploited active materials for the photovoltaic conversion of solar energy.[8−10] The potential for the application of oligothiophenes in medicine and biology is also noteworthy because of their designer's electronic, optical, and redox properties. In fact, the orbital energies of oligothiophenes can be regulated by selectively introducing electron donating (D) and accepting (A) groups. This strategy has been used to design molecules, polymers, and nanoparticles for electronic and biological applications.[11−18] Recent studies showed the possibility of using oligothiophene fluorophores for proteins and DNA labeling and for the staining of cells.[19−23] Oligothiophenes were also used as tools for pathological and prognostic evaluation of neurological diseases and to interact with cells and complex organisms.[24−27] Further uses of thiophene derivatives can be sought in view of

Received: February 11, 2021
Published: July 6, 2021

https://doi.org/10.1021/jacsau.1c00061
JACS Au 2021, 1, 925–935

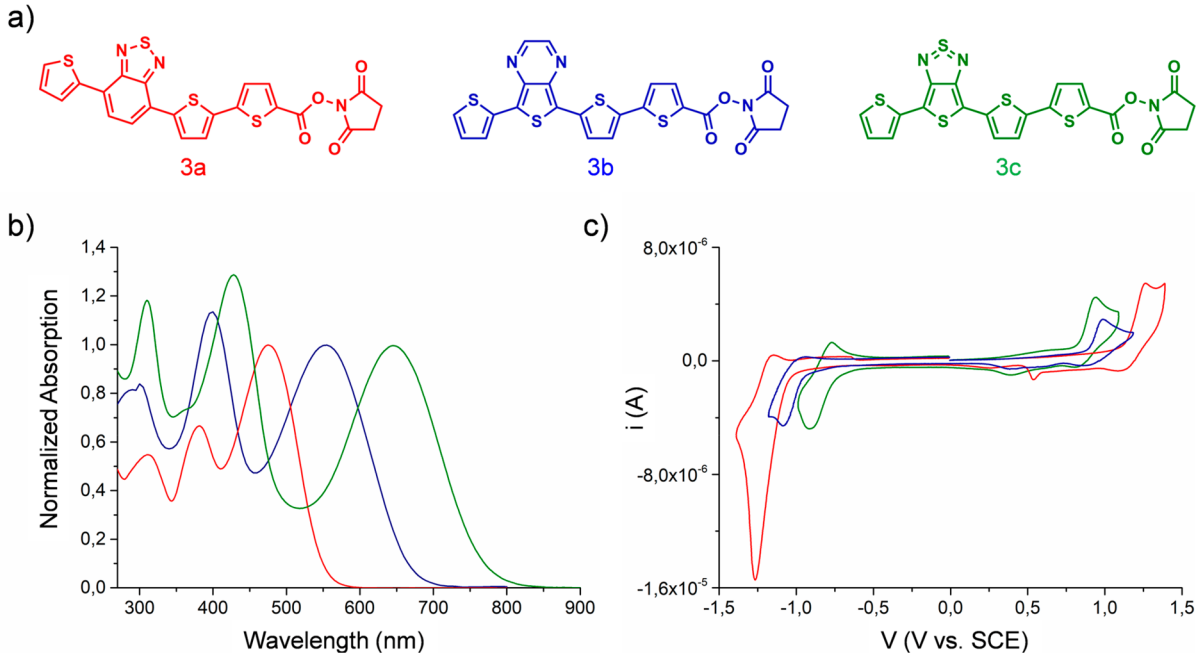

Figure 1. (a) Molecular structures of the oligothiophene *N*-hydroxysuccinimidyl esters **3a**, **3b**, **3c**. (b) UV−vis spectra of the compounds **3a** (red line), **3b** (blue line), **3c** (green line) in DMF. The spectra are normalized to the absorption band relative to the lowest energy transition of each molecule. (c) Voltammograms of **3a** (red line), **3b** (blue line), **3c** (green line) in $CH_2Cl_2$0.1 mol·L^{-1} $(C_4H_9)_4NClO_4$ on Pt disk electrode (1 mm diameter, scan rate 0.1 v s^{-1}).

the success that π-conjugated systems have achieved as light-activated heat generators for photothermal therapy (PTT) and as reactive oxygen species (ROS) producers for photodynamic therapy (PDT).[28−33] PDT is a minimally invasive therapeutic modality approved for clinical treatment of several types of cancer.[34,35] In PDT, a compound with photosensitizing properties (the photosensitizer or PS) is accumulated in target cells. The activation of the PS by light, in the presence of oxygen, generates ROS that are cytotoxic for the neoplastic cells.[36−38] Image-guided PDT represents a new frontier in PDT treatments.[39−42] The agents that are used as photosensitizers for PDT can also serve for fluorescence image-guided surgery (FGS) and thus mediate fluorescence imaging. Currently, there are only four FDA-approved contrast agents for FGS, namely, fluorescein, indocyanine green, 5-aminolevulinic acid, and methylene blue.[40] Many FGS contrast agents are currently undergoing clinical trials. They are characterized by an incredible variety of molecular types, targeting mechanisms, and fluorescence properties. The bottleneck to reach clinical use is represented by the fact that FGS contrast agents are considered new drugs by the FDA and face a lengthy and expensive approval process.[40] Crucially, light emission (required for image-guided PDT) and photosensitization (required for ROS generation) are competing processes.[39] Imaging techniques alternative to fluorescence, such as photoacoustics,[41] magnetic resonance, or nuclear imaging, can also be adopted to develop innovative image-guided PDT platforms.[42]

The intrinsic properties of a PS determine its therapeutic efficiency.[43,44] There are many requirements for the design of a good PS: proper absorption wavelength, high absorptivity, high stability under photoirradiation and in physiological conditions, low levels of dark toxicity, and high levels of accumulation in tumor tissues.[39,43,44]

Oligothiophenes meet all the photophysical requirements of an optimal PS, but they are commonly used in nanoparticle formulation,[45−48] because in molecular form, their intrinsic hydrophobicity lowers their biocompatibility and availability in water where they have a high tendency toward aggregation.[49] The delivery of hydrophobic PS to the tumor cells is still an important limit to face in PDT.[50,51] The binding of hydrophobic PS molecules to a protein/peptide can overcome the limitations regarding their use in physiological environments.[52−56] Albumins, in particular, are promising carriers for drugs[57,58] and photosensitizers[59−61] due to their inherent nonimmunogenicity, biocompatibility, and biodegradability. Human serum albumin (HSA), a long-circulating and highly abundant protein in the blood, is a promising carrier for cancer therapeutics: (i) it is the natural carrier of hydrophobic molecules in the blood, (ii) it is rescued from systemic clearance and degradation by natural mechanisms, (iii) it accumulates at sites of vascular leakiness such as cancer tissues, and (iv) its uptake is high in rapidly growing, nutrient-starved cancer cells.[62,63]

Herein, we present novel amino-reactive quaterthiophenes functionalized with different acceptor groups of varying strength, easily conjugable to HSA. The conjugation with HSA allows solubilization of the oligothiophenes in water, while preserving the biological identity of the protein. The bioconjugate produced is fluorescent and biocompatible, and facilitates cellular trafficking and membrane interactions. We demonstrate that HSA−oligothiophene bioconjugation offers the possibility to be used *per se* as a multifunctional theranostic platform with both therapeutic and imaging properties. Indeed, we show that the bioconjugate, upon irradiation with ultralow light doses, is able to (i) efficiently generate reactive oxygen species (ROS) leading to the complete and localized eradication of cancer cells and (ii) provide detailed cell-imaging.

https://doi.org/10.1021/jacsau.1c00061
JACS Au 2021, 1, 925−935

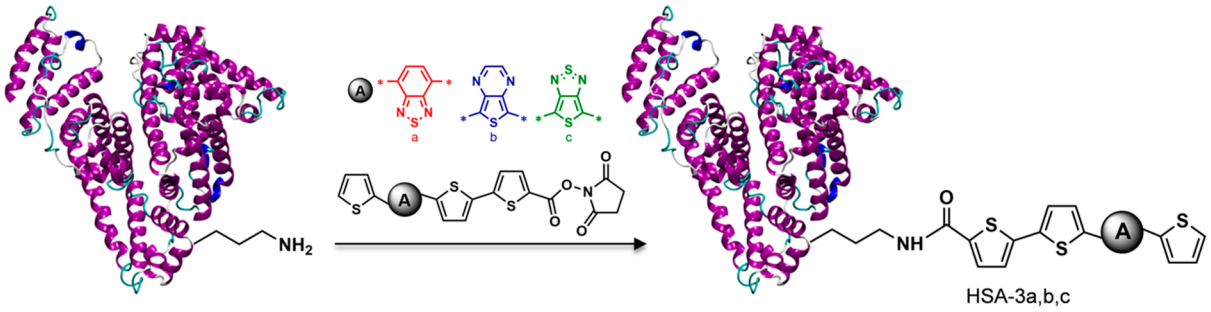

Figure 2. Conjugation of oligothiophene *N*-hydroxysuccinimidyl esters, NHS, to HSA.

RESULTS AND DISCUSSION

Synthesis and Characterization of Oligothiophene *N*-Hydroxysuccinimidyl Esters

The introduction of donor and acceptor units into thiophene-based materials (donor−acceptor−donor, i.e., DAD structures) allows one to tune the HOMO−LUMO energy levels, which further control the absorption wavelengths, the performance as a photosensitizer, and the fluorescence quantum yield. These properties are also crucial for imaging applications. In this context, three different DAD oligothiophenes **3a−c** (Figure 1a) were prepared by alternating bromination and cross-coupling reactions (see SI for details, Figures S1−S4). They are characterized by identical donor units, constituted of thiophene moieties, and acceptor groups of increasing strength, namely, benzothiadiazole, thienopyrazine, and thienothiazole. A succinimidyl ester (NHS) moiety was linked to the dyes to allow bioconjugation with proteins. Protein conjugation is a general strategy that can improve solubility of hydrophobic PS in physiological environments.

As expected, upon increasing the strength of the acceptor group, the UV−vis absorption spectrum shifts toward longer wavelengths (Figure 1b), going from 474 nm for compound **3a** (benzothiadiazole as acceptor) to 550 nm for compound **3b** (thienopyrazine as acceptor) and to 644 nm for compound **3c** (thienothiadiazole as acceptor). The emission spectra of these compounds follow the same order as the absorption ones, since **3c** (868 nm) is more red-shifted than **3b** (710 nm) and **3a** (644 nm) (Figure S8 and Table S2). As a result, compounds **3a** and **3b** show smaller Stokes shifts than **3c** suggesting a more planar conformation for these two oligomers, in accordance with the trend of the molar absorption coefficients (Table S2). Cyclic voltammetries agree with optical measurements (Figures 1c, S5−S7, Table S1) and show that upon increasing the strength of the central acceptor moiety, the HOMO−LUMO energy gap is reduced. The three voltammograms (Figure 1c) present quasi-reversible oxidation and reduction waves. The oxidation potentials decrease following the trend **3a** > **3b** > **3c**, in agreement with the lower excitation energy of the thienopyrazine unit compared to the benzothiadazole one that favors the formation of the radical-cation.[64−66] On the contrary, the reduction potentials increase following the order **3a** < **3b** < **3c** revealing a gradually decreasing π-electron length of the LUMO. All the measurements were carried out in DMF/CH_2Cl_2, because the molecules are insoluble in water.

Synthesis and Characterization of HSA−Oligothiophene Bioconjugates

The oligothiophenes were conjugated to Human Serum Albumin, HSA. The HSA−oligothiophene conjugates were synthesized via cross-coupling reaction between NHS moiety of the oligothiophenes derivatives and amino acid amine groups of HSA (Figure 2). Protein conjugation makes the molecules highly soluble in water, and the bioconjugates were characterized in PBS.

Absorption spectra of the purified HSA−oligothiophene bioconjugates displayed a red-shift when compared to nonconjugated oligothiophenes (Figure S8). These changes in the absorption spectra, and in the photophysical parameters (Table S2), confirmed the attachment of the dyes to HSA. The HSA−oligothiophene bioconjugates largely retain their emission quantum yields (φ_{Em}) and possess large Stokes shifts, which are attractive photophysical properties for imaging applications. Considering the initial HSA concentration and the molar extinction coefficients of the three oligothiophenes **3a**, **3b**, and **3c**, approximately 1.5, 1.0, and 2.2 molecules were conjugated per HSA protein. Electrophoretic measurements are consistent with the attachment of the dyes to the protein (Figure S9). DLS characterization of the HSA bioconjugates (Figure S10) confirms that the coupling procedure preserves HSA in the physiological monomeric form. Circular dichroism (CD) spectra (Figure S11) indicate that HSA maintains its native folding upon conjugation with the oligothiophenes.

ROS Generation Ability of HSA-3a Bioconjugate in PBS Buffer

The ability of HSA−oligothiophene bioconjugates to behave as photosensitizers, upon irradiation with visible light in the physiological environment, was evaluated using the ABMDMA assay to detect $^1O_2$ and the Amplex Red assay (Figure 3) to detect peroxides.

The disodium salt of ABMDMA (9,10-anthracenediyl-bis(methylene)dimalonic acid) reacts with $^1O_2$ to give an endoperoxide. This reaction is detected by the bleaching of ABMDMA, measuring the decline of its absorbance at 401 nm. Colorless, nonfluorescent Amplex Red, reacts with peroxides to form colored, fluorescent resorufin, catalyzed by horseradish peroxidase (HRP) enzyme. The concentration of the produced peroxides is proportional to the generated resorufin (see SI for details).

Upon visible light irradiation, compound **3a** generates both peroxides and $^1O_2$. No ROS generation was detected for compounds **3b** and **3c**. The singlet oxygen quantum yield ($\Phi\Delta$) of **HSA-3a** was calculated using free Rose Bengal (RB) as a reference. **$\Phi\Delta$-HSA-3a** is 0.19 to be compared with a value of Φ_Δ-RB of 0.76.[67] To investigate the excited states of the bioconjugates (S_1 and T_1), we conducted time-dependent density functional theory (TD-DFT) calculations using the Gaussian 16 package (see SI for details). Jablonsky diagrams explain the reason only **HSA-3a** generates $^1O_2$. In fact, in

https://doi.org/10.1021/jacsau.1c00061
JACS Au 2021, 1, 925−935

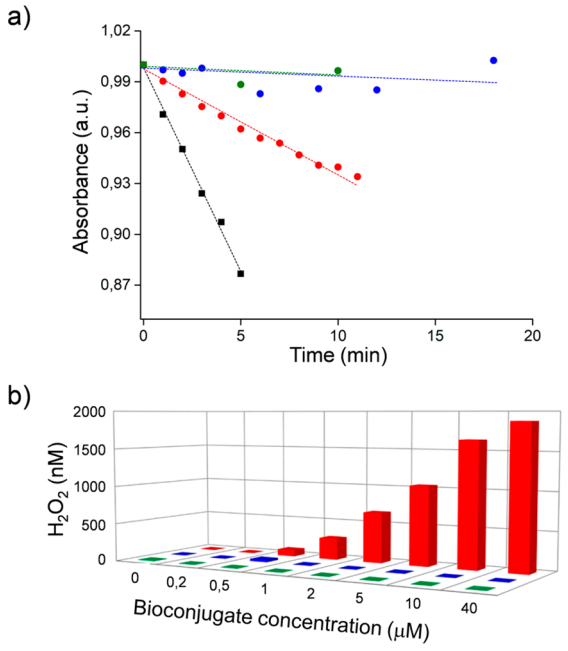

Figure 3. (a) Decrease of ABMDMA absorbance vs irradiation time under 555 nm irradiation for **HSA-3a** (red), **HSA-3b** (blue), and **HSA-3c** (green), rose bengal (black). (b) Generation of peroxides during visible light irradiation, using different concentrations of **HSA-3a** (red), **HSA-3b** (blue), and **HSA-3c** (green).

compounds **3b** and **3c** the lowest triplet state is located below the singlet oxygen state (Figure 4).

Cytotoxicity and Phototoxicity of HSA-3a Bioconjugate in HeLa Cells

The cytotoxicity and the potential phototoxicity of the bioconjugate **3a** were assessed by *in vitro* experiments employing HeLa cells, a human cancer cell line.

Figure 5 shows that no reduction of cell viability was observed for cells kept in dark conditions, even if they were incubated with high concentrations of the bioconjugate photosensitizer (up to 50 μM). This result demonstrates that **HSA-3a** is biocompatible and does not have any "dark toxicity". In contrast, after incubation with the bioconjugate, HeLa cells irradiated with visible light even at ultralow light dose (2.4 mW/cm^2) showed a dose-dependent decrease of viability (Figure 5).

The photocytotoxicity depends on the concentration of the photosensitizer, present in the cell medium during incubation ($IC_{50} \approx 1$ μM). At 2 μM of the bioconjugate, 100% of the cultured HeLa cells died after photoirradiation.

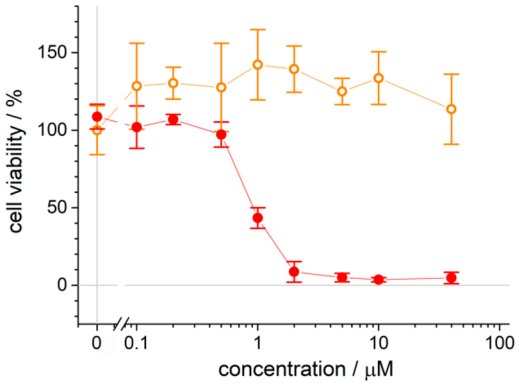

Figure 5. Phototoxicity of the **HSA-3a** bioconjugate on HeLa cells upon photoirradiation. Cell viability in dark conditions (orange open circles) or upon visible light irradiation (red filled circles) at different **HSA-3a** concentrations. Each value represents the average ± 1 standard deviation of 3 independent measurements.

Cellular Uptake of the HSA-3a Bioconjugate in HeLa Cells

It is possible to image the cellular localization of **HSA-3a** bioconjugate exploiting its intrinsic fluorescence (Figure 6).

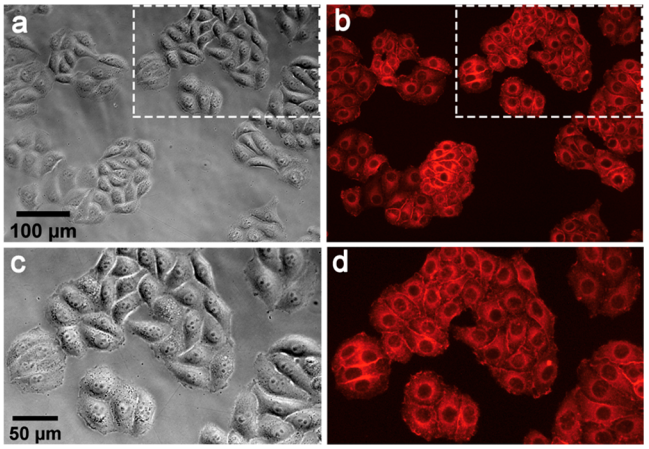

Figure 6. HSA-3a internalization by HeLa cells: (a, c) bright field images, (b, d) fluorescence images obtained by irradiation with a mercury lamp filtered with a Nikon TRITC cubic filter ($\lambda_{excitation}$ = 520−570 nm, $\lambda_{emission}$ = 580−640 nm; see Methods for details), (c, d) magnifications of the region indicated by white rectangles of (a) and (b), respectively.

Fluorescence images of the HeLa cells incubated with **HSA-3a** bioconjugate show red fluorescence localized in the cellular membrane and in the cytoplasm. **HSA-3a** bioconjugate offers the possibility to be used *per se* as a theranostic platform,

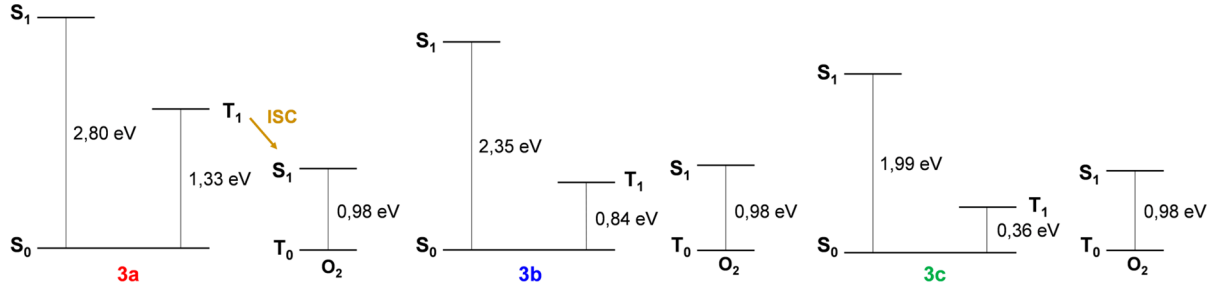

Figure 4. TD-DFT calculations of singlet and triplet low-lying levels of **3a**, **3b**, and **3c** together with the comparison with the oxygen levels.

https://doi.org/10.1021/jacsau.1c00061
JACS Au 2021, 1, 925−935

because it combines the possibility to generate ROS with imaging opportunities. The system appears to be an outstanding candidate for image-guided PDT applications.

Real-Time Monitoring of the Photokilling Activity of HSA-3a

To investigate in detail the photokilling activity of **HSA-3a**, HeLa cells were imaged real-time by confocal microscopy during irradiation (Figure 7). Time lapse imaging of the HeLa

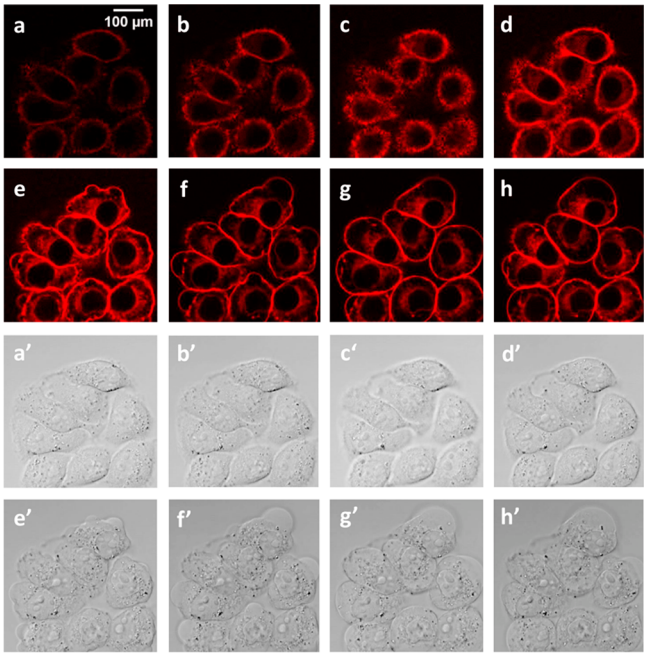

Figure 7. Real-time monitoring of the photokilling activity of HeLa cells upon **HSA-3a** irradiation. Panels (a–h) (fluorescence images) and (a′–h′) (bright field images) were extracted from a time lapse of 7 min every 176 s; cells were exposed to 488 nm laser light during confocal fluorescence image collection every 2 s.

cells, exposed to 488 nm laser light, showed membrane blebbing on the cells during irradiation. Membrane blebbing is a morphological characteristic of oxidative stress and also one feature of apoptosis induced by PDT treatment.[68,69] Apoptosis induction by PDT has been already described.[70] Different mechanisms of apoptosis triggering by PDT are known.[70] Interestingly, thanks to the intrinsic fluorescence of the oligothiophenes and to the accumulation of **HSA-3a** in the cellular membrane, all the investigations are stain-free, and **HSA-3a** behaves as a real-time self-reporting system to monitor the apoptotic process. Figure 7 shows the "explosion" of the cells upon irradiation.

Photostimulation of Apoptosis upon HSA-3a Irradiation

Flow cytometry analysis of Annexin V staining was performed (Figure 8). It facilitated determination of whether photostimulation by **HSA-3a** induced apoptosis.

No induction of apoptosis was detected in cells kept under dark conditions, even at high **HSA-3a** bioconjugate concentrations. Conversely, a photodependent and dose-dependent increase in the percentage of apoptotic cells was observed by incubating cells with increasing doses of **HSA-3a**. Collectively, these proofs indicate that apoptosis is one of the primary mechanisms of cell death activated by **HSA-3a** irradiation.

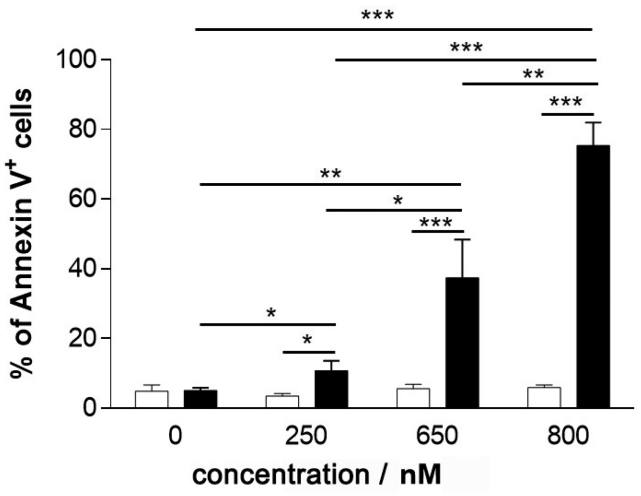

Figure 8. Photoinduced apoptosis in HeLa cells upon irradiation of **HSA-3a**. HeLa cells were treated with increasing **HSA-3a** bioconjugate concentrations for 3 h, then exposed to light for 10 min (black histograms) or kept in the dark (white histograms). Cells were then cultured for an additional 24 h after drug washout. The percentage of Annexin V+ cells was reported as mean ± 1 standard deviation of 3 independent experiments (* $p < 0.05$, ** $p < 0.01$, *** $p < 0.001$).

Localized Killing of HeLa Cells by HSA-3a Bioconjugate by Precise Light Activation

To investigate the possibility of performing highly spatially controlled killing of cells by light activation, PDT treatment of 2D cultures was performed by irradiating the cells directly under a microscope. The optics of the microscope were regulated in order to obtain a well-defined irradiation spot (Figure 9a,b) on the of 2D cell culture (Figure 9c). The resulting PDT efficacy was evaluated through live/dead staining (calcein-AM/propidium iodide). The experiments showed that there are no signs of cellular death in the non-irradiated region (Figure 9d, green fluorescence). On the other hand, PDT treatment caused substantial cellular death solely in the irradiation spot (Figure 9e, red fluorescence). Figure 9f demonstrates the precise localization of the killing. In general, ROS have a very short diffusion path; **HSA-3a** generates ROS; the localized killing is therefore likely due to oxidative stress that is spatially produced and confined to the irradiated region.

Intracellular Reactive Oxygen Species (ROS) Production in HeLa cells upon Illumination of HSA-3a

Finally, in order to further test the photoactivity of **HSA-3a** bioconjugated, we monitored the intracellular formation of reactive oxygen species (ROS) upon illumination of **HSA-3a** in HeLa cells by using 2′,7′-dichlorofluorescin diacetate (DCHF-DA) as a reporter (see Methods for details on sample preparation).

DCFH-DA is a molecule able to permeate the cell membrane, where it is hydrolyzed by the cellular esterases to DCFH, which, in the presence of intracellular ROS, it is oxidized to the highly fluorescent DCF. The fluorescence intensity of DCF in the cells is an indirect measure of ROS formation.

Localized illumination experiments on HeLa cells loaded with DCHF-DA in the presence or in the absence of **HSA-3a** (Figure 10) clearly demonstrate the formation of reactive oxygen species in the cell cytoplasm only when **HSA-3a** and

https://doi.org/10.1021/jacsau.1c00061
JACS Au 2021, 1, 925–935

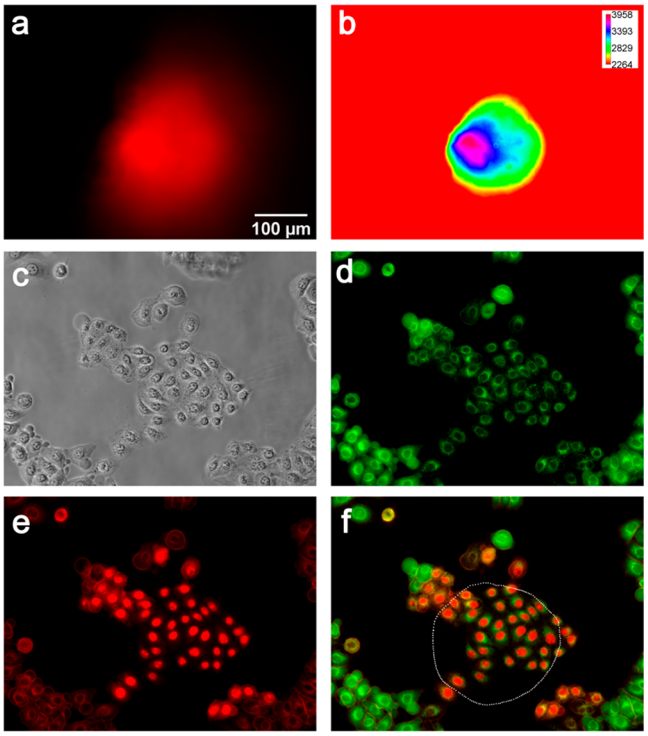

Figure 9. Localized photokilling of HeLa cells. HeLa cells were irradiated for 10 min with a mercury lamp filtered using a Nikon Texas Red HYQ cubic filter ($\lambda_{excitation}$ = 532−587 nm, $\lambda_{emission}$ = 608−683 nm; see Methods for details). (a, b) Dimensions of the irradiation spot, represented by a red (a) and by an intensity spectrum (b); the calibration bars of light intensity are reported in relative units. (c) Phase contrast image after irradiation. (d) Green fluorescence ($\lambda_{excitation}$ = 465−495 nm, $\lambda_{emission}$ = 515−555 nm; see Methods for details) signal is due to the staining of living cells with calcein-AM. (e) Red fluorescence ($\lambda_{excitation}$ = 532−587 nm, $\lambda_{emission}$ = 608−683 nm) is due to the staining of nuclei of died cells with propidium iodide. (f) Overlay of red (e) and green (d) channels; approximation of irradiation spot boundaries is shown as a white dotted line.

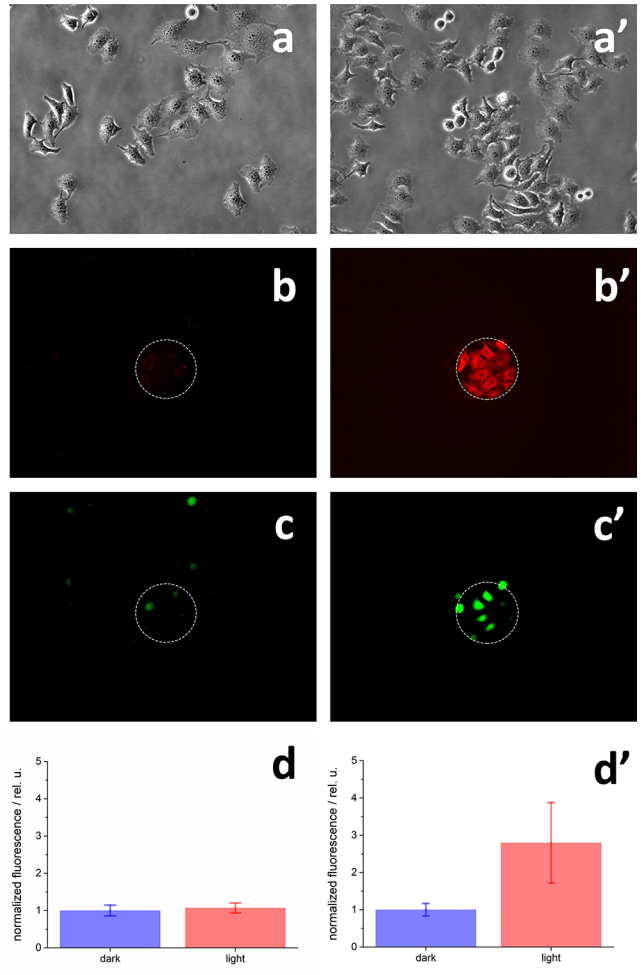

Figure 10. Reactive oxygen species (ROS) production in HeLa cells upon illumination of HSA-3a. (a−d): cells incubated with 100 μM DCHF-DA; (a′−d′): cells incubated with 800 nM **HSA-3a** and 100 μM DCHF-DA (see Methods for details). (a,a′) HeLa cells before illumination loaded with (a) 100 μM DCHF-DA or (a′) 100 μM DCHF-DA and 800 nM **HSA-3a**; any dead cell can be detected before localized illumination. (b,b′) 10 s illumination with green light ($\lambda_{excitation}$ = 532−587 nm, $\lambda_{emission}$ = 608−683 nm). Illumination was confined to the area indicated with the dashed white circle; (c,c′) DCHF-DA fluorescence taken 10 s after 10 s illumination with green light. Images were obtained using a Nikon FITC cubic filter ($\lambda_{excitation}$ = 465−495 nm, $\lambda_{emission}$ = 515−555 nm; see Methods for more information). Fluorescence images were measured with an intensity scale 1−4092 (12 bit); LUT scales for c and c′ panels were all set with minimum−maximum values of 180−321; (d,d′) quantification of DCHF-DA fluorescence signals for illuminated (light, red) and non-illuminated (dark, blue) cells. Bars and error bars are the average and standard deviation values of mean intensity fluorescence signals as detailed in the Methods section; normalized fluorescence values were obtained by dividing each value for the average fluorescence intensity measured for non-illuminated cells (i.e., cells outside of the white dashed circle of panel b,b′).

light are present; a 3-fold increase of DCHF-DA signal reports a corresponding increase of ROS as a consequence of 10 s illumination with green light (532−587 nm) for HeLa cells incubated with **HSA-3a**.

CONCLUSIONS

Three different DAD oligothiophenes, characterized by donor and acceptor groups of increasing strength, were synthesized. Upon increasing the strength of the acceptor group, the HOMO−LUMO energy gap is reduced as confirmed by UV−vis absorption spectrum and cyclic voltammetries. A succinimidyl ester (NHS) moiety was linked to the dyes. HSA−oligothiophene conjugates were then synthesized via cross-coupling reaction between NHS and amino acid amine groups of HSA. Protein conjugation made the dye molecules highly soluble in water. UV−vis, electrophoresis, and dynamic light scattering confirmed the attachment of the oligothiophenes to the protein, preserving HSA in the physiological monomeric form. Upon visible light irradiation, one of the bioconjugates was highly active in the generation of both peroxides and $^1O_2$. The different behavior of the three oligothiophenes was explained by DFT calculations. The PDT performances of the HSA−oligothiophene bioconjugate was assessed *in vitro* with HeLa cells. The HSA−oligothiophene bioconjugate is biocompatible and does not show any "dark toxicity". In contrast, when the cells were irradiated, even with ultralow-dose visible light, a dose-dependent decrease of HeLa cells viability was observed ($IC_{50} \approx 1$ μM). By exploiting the intrinsic fluorescence of the bioconjugate, it was also possible to image its cellular localization in the cellular membrane and in the cytoplasm. The photokilling activity of HSA−oligothiophene was

https://doi.org/10.1021/jacsau.1c00061
JACS Au 2021, 1, 925−935

investigated by real-time imaging of the HeLa cells by confocal microscopy carried out in the presence of irradiation. Time-lapse imaging showed the "explosion" of the cells upon irradiation. Again, because of the intrinsic fluorescence of the oligothiophenes and the accumulation of HSA−oligothiophene in the cellular membrane, all the investigations were stain-free. The bioconjugate behaves as a real-time self-reporting system. Flow cytometry analysis indicated that cell apoptosis is one of the primary causes of the effective killing process by HSA−oligothiophene irradiation. The induction of apoptosis is photodependent and dose-dependent.

Localized killing of cancer cells by precise light activation was observed by focusing the irradiation spot: no signs of cellular death were observed in the non-irradiated region, while PDT treatment caused substantial cellular death in the irradiation spot. Intracellular reactive oxygen species (ROS) production in HeLa cells upon illumination of **HSA-3a** was demonstrated.

HSA-3a bioconjugate offers the possibility to be used *per se* as a theranostic platform. In the future, we foresee HSA−oligothiophene bioconjugates being employed as photo-theranostic agents in vivo for image-guided PDT.

Considering the properties of oligothiophenes and their applications in nanomedicine,[17] HSA−oligothiophene bioconjugates can be potentially used also in photothermal therapy[71,72] and optoacoustic imaging.[71,72] The platform can also be excited by two-photon excitation,[66] which should bring important benefits to PDT, increasing the treatment penetration depth with NIR light excitation, improving the spatial selectivity, and reducing photodamage of healthy tissues.[73] Finally, the different chemical groups present in the protein platform can afford an easy route for additional functionalization of the hybrid. In this way, the performances of the bioconjugate platform can be improved, for instance, by using targeting tags able to enhance cell selectivity and promote the uptake of the bioconjugate in cancer cells or by conjugating the oligothiophene molecule to other carrier proteins/antibodies. The application field of the bioconjugates can also be easily expanded to antimicrobial photodynamic therapy.[74]

METHODS

HSA−Oligothiophene Synthesis and Purification

N-Hydroxysuccinimidyl esters of oligothiophenes **3a**, **3b**, and **3c** were dissolved in dimethylformamide (DMF) at a concentration 5 mM. 50 μL of these solutions were slowly added dropwise to 1 mL of HSA 20 μM in sodium carbonate buffer 100 mM pH 9 under vigorous stirring.

The reaction was incubated overnight in the dark, under mild stirring condition, and then it was centrifuged at 14000g, for 10 min to remove the insoluble excess of nonconjugated oligothiophene derivatives. The samples were then extensively dialyzed against PBS 10 mM pH 7.4, in cellulose membrane dialysis tubes with a 14 KD cutoff, to remove the water-soluble byproducts generated during the coupling procedure.

Cell Cultures

The human cervical adenocarcinoma (HeLa, ATCC) cell line was used as an *in vitro* model. Cells were cultured in Dulbecco's Modified Eagle's Medium (DMEM) supplemented with 10% fetal bovine serum (FBS) South America, 2 mM L-glutamine, and 50 U/mL penicillin/50 μg/mL streptomycin; the sterile culturing medium was filtered by means of 0.20 μm filters (Millipore) just before use. Cells were grown in an incubator at 37 °C, 5% CO_2, and were passed upon trypsin digestion every 3 days.

In Vitro Measurement of Cytotoxicity and Photodynamic Activity of HSA-3a in HeLa Cells

To measure the photodynamic activity of **HSA-3a**, HeLa cells were plated at a density of 5×10^3 cells per well in 96-well plates. The cells were incubated for 3 h in dark condition with several concentrations of the **HSA-3a** bioconjugate (0, 0.1 μM, 0.2 μM, 0.5 μM, 1 μM, 2 μM, 5 μM, 10 μM, 40 μM); after the incubation, the cells were washed with phosphate-buffered saline (PBS). Half of the dishes were exposed to the light source (a white LED Valex 30 W at 30 cm distance from the cell-plate; irradiation power density on the cell plate = 2.4 mW/cm^2: measured with the photoradiometer Delta Ohm LP 471 RAD) for 10 min in PBS, while the other dishes were left in the presence of PBS in dark conditions. After treatment, PBS was replaced with the standard culture medium, and all the samples were incubated for 24 h at 37 °C, 5% CO_2; the cell viability was then assessed, using MTT assay (Merck, product no. M2128), both for the samples which were irradiated and for the ones kept in dark conditions. The data are reported as the mean value ± standard deviation (SD) of 3 to 6 different replicates.

Cellular Uptake of the HSA-3a Bioconjugate in HeLa Cells

HeLa cells were plated at 5×10^4 cells in a 3.5 cm Petri dishes and incubated with 5 μM **HSA-3a** in complete medium for 1 h. After washing with PBS, red fluorescence images were acquired with a Nikon TiS widefield fluorescence microscope equipped with a TRITC cubic filter (λ excitation = 520−570 nm, λ emission = 580−640 nm).

Real-Time Monitoring of the Photokilling Activity of HSA-3a

Petri dishes (3.5 cm diameter) were seeded with 5×10^4 cells and after adhesion incubated with 5 μM **HSA-3a** in complete medium for 1 h. Before acquiring images, **HSA-3a** not internalized by cells was removed by washing samples with PBS. Confocal time lapses were obtained with an Olympus FLUOVIEW FV3000 confocal microscope; **HSA-3a** was excited at 488 nm with a laser diode and fluorescence revealed in the 550−650 nm range; image acquisition was set at 1 Hz.

Photostimulation of Apoptosis upon HSA-3a Irradiation

HeLa cells were seeded at a density of 3.3×10^4 cells per well in 24-well plate, at a final concentration of 5×10^4/mL. After 24 h, cells were treated with increasing concentrations of **HSA-3a** (0, 250, 650, 800 nM) for 3 h, then exposed to the light source for 10 min in PBS (or dark condition fron control cells), and then cultured in standard medium for additional 24 h after drug washout. Cells were harvested by trypsin digestion, and phosphatidyl serine externalization was evaluated using the fluorescein isothiocyanate (FITC) Annexin V Apoptosis Detection Kit (eBioscience Thermo Fisher Scientific) according to the manufacturer's instruction. The percentage of apoptotic cells (Annexin V$^+$) was determined by flow cytometry (Facs Canto II Flow Cytometer, BD Biosciences Pharmingen, California, US). Values represent the mean ± standard deviation of three independent experiments. Multiple comparisons were performed using two-way analysis of variance with Bonferroni post-hoc test (***$p < 0.001$).

Localized Killing of HeLa Cells by HSA-3a Bioconjugate by Precise Light Activation

HeLa cells were plated in 3.5-cm-diameter Petri dishes at a density of 4×10^4 cells per well. The following day, cells were incubated with 5 μM **HSA-3a** in complete medium for 1 h; cells were washed in PBS supplemented with calcium and magnesium (ThermoFisher, product no. 14040091) and then kept in HBSS (Hanks Balanced Salt Solution medium, Merck, product no. H8264) in the dark. Cells were illuminated for 10 min with a mercury lamp filtered using a Nikon Texas Red HYQ cubic filter ($\lambda_{excitation}$ = 532−587 nm, $\lambda_{emission}$ = 608−683 nm; power density measured at 550 nm − 70 mW/mm^2). After illumination, cells were washed with PBS and incubated for 30 min with 4 μM calcein−AM e 4 μM propidium iodide in HBSS (calcein−AM, ThermoFisher product no. C1430; propidium iodide, Merck product no. P4864). After incubation, cells were washed with PBS,

https://doi.org/10.1021/jacsau.1c00061
JACS Au 2021, 1, 925−935

and the fluorescence images were recorded using a Nikon TiS fluorescence microscope. Red fluorescence from propidium iodide and **HSA-3a** was detected employing a Nikon Texas Red HYQ cubic filter ($\lambda_{excitation}$ = 532−587 nm, $\lambda_{emission}$ = 608−683 nm), while using calcein−AM green fluorescence using a Nikon FITC cubic filter ($\lambda_{excitation}$ = 465−495 nm, $\lambda_{emission}$ = 515−555 nm).

Intracellular Reactive Oxygen Species (ROS) Production in HeLa Cells upon Illumination of HSA-3a Bioconjugate

2′,7′-Dichlorofluorescin diacetate (DCHF-DA) was purchased from Merck-Sigma-Aldrich (product number D6883); fresh 10 mM DCHF-DA solution in dimethyl sulfoxide was prepared before experiments. HeLa cells were seeded overnight in complete growth medium in Petri dishes with a 3.5 cm diameter; 6×10^4 HeLa cells were plated in each dish. Each sample was incubated for 1 h with 800 nM **HSA-3a** in the complete medium; after removing the medium with **HSA-3a**, cells were washed with PBS and incubated for 30 min with 100 μM DCHF-DA in HBSS in the incubator. Cells were then further washed with PBS and supplemented with fresh HBSS before fluorescence experiments were performed.

Localized illumination experiments were performed with a Nikon TiS fluorescence microscope equipped with a FITC cubic filter ($\lambda_{excitation}$ = 465−495 nm, $\lambda_{emission}$ = 515−555 nm) and a Nikon Texas Red HYQ cubic filter ($\lambda_{excitation}$ = 532−587 nm, $\lambda_{emission}$ = 608−683 nm); during the 10 s illumination, the Texas Red HYQ cubic filter was employed and approximately 20 mW/mm^2 was directed to the illuminated cells.

Quantification of DCHF-DA fluorescence was obtained with Fiji ImageJ software;[75] mean intensities of the region of interests (ROI) were manually calculated for illuminated and not illuminated cells, i.e., cells, respectively, inside and outside the white dashed circle of Figure 10c,c′. The following number of ROI was measured: Figure 10c, 23 ROIs in the dark and 4 ROIs in the light; Figure 10c′, 42 ROIs in the dark and 14 ROIs in the light. Average and standard deviation values were calculated for each population. Normalized fluorescence intensities of Figures 10 were obtained by dividing each average and standard deviation values for the average value of ROI fluorescence mean intensity measured for not illuminated cells of the corresponding image. The experiment is representative of three replicas.

■ ASSOCIATED CONTENT

Supporting Information

The Supporting Information is available free of charge at https://pubs.acs.org/doi/10.1021/jacsau.1c00061.

> Oligothiophene *N*-hydroxysuccinimidyl esters synthesis; Oligothiophene *N*-hydroxysuccinimidyl esters characterization: ^{1}H NMR; Mass spectra; Cyclic Voltammetries. Materials, HSA−oligothiophene characterization (photophysical measurements; electrophoresis; dynamic light scattering; circular dichroism, Amplex Red peroxides quantification; ABMDMA singlet oxygen assay). Computational details. (PDF)

■ AUTHOR INFORMATION

Corresponding Authors

Stefania Rapino − *Dipartimento di Chimica "Giacomo Ciamician, Alma Mater Studiorum, Università di Bologna, 40126 Bologna, Italy;* orcid.org/0000-0001-6913-0119; Email: stefania.rapino3@unibo.it

Francesca Di Maria − *Istituto per la Sintesi Organica e la Fotoreattività (ISOF), Consiglio Nazionale delle Ricerche, 40129 Bologna, Italy; Mediteknology srl, 40129 Bologna, Italy;* orcid.org/0000-0001-5557-3816; Email: francesca.dimaria@isof.cnr.it

Matteo Calvaresi − *Dipartimento di Chimica "Giacomo Ciamician, Alma Mater Studiorum, Università di Bologna, 40126 Bologna, Italy;* orcid.org/0000-0002-9583-2146; Email: matteo.calvaresi3@unibo.it

Authors

Andrea Cantelli − *Dipartimento di Chimica "Giacomo Ciamician, Alma Mater Studiorum, Università di Bologna, 40126 Bologna, Italy*

Marco Malferrari − *Dipartimento di Chimica "Giacomo Ciamician, Alma Mater Studiorum, Università di Bologna, 40126 Bologna, Italy*

Alice Soldà − *Dipartimento di Chimica "Giacomo Ciamician, Alma Mater Studiorum, Università di Bologna, 40126 Bologna, Italy*

Giorgia Simonetti − *IRCCS Istituto Romagnolo per lo Studio dei Tumori (IRST) "Dino Amadori", 47014 Meldola, FC, Italy*

Sonny Forni − *Dipartimento di Chimica "Giacomo Ciamician, Alma Mater Studiorum, Università di Bologna, 40126 Bologna, Italy*

Edoardo Toscanella − *Dipartimento di Chimica "Giacomo Ciamician, Alma Mater Studiorum, Università di Bologna, 40126 Bologna, Italy*

Edoardo J. Mattioli − *Dipartimento di Chimica "Giacomo Ciamician, Alma Mater Studiorum, Università di Bologna, 40126 Bologna, Italy*

Francesco Zerbetto − *Dipartimento di Chimica "Giacomo Ciamician, Alma Mater Studiorum, Università di Bologna, 40126 Bologna, Italy;* orcid.org/0000-0002-2419-057X

Alberto Zanelli − *Istituto per la Sintesi Organica e la Fotoreattività (ISOF), Consiglio Nazionale delle Ricerche, 40129 Bologna, Italy*

Matteo Di Giosia − *Dipartimento di Chimica "Giacomo Ciamician, Alma Mater Studiorum, Università di Bologna, 40126 Bologna, Italy;* orcid.org/0000-0003-3494-298X

Mattia Zangoli − *Istituto per la Sintesi Organica e la Fotoreattività (ISOF), Consiglio Nazionale delle Ricerche, 40129 Bologna, Italy; Mediteknology srl, 40129 Bologna, Italy;* orcid.org/0000-0002-0340-9245

Giovanna Barbarella − *Istituto per la Sintesi Organica e la Fotoreattività (ISOF), Consiglio Nazionale delle Ricerche, 40129 Bologna, Italy; Mediteknology srl, 40129 Bologna, Italy*

Complete contact information is available at: https://pubs.acs.org/10.1021/jacsau.1c00061

Notes

The authors declare no competing financial interest.

■ ACKNOWLEDGMENTS

Igor Del Vecchio is gratefully acknowledged for technical support in time lapse acquisition with the Olympus FLUOVIEW FV3000 confocal microscope. M.D.G. was supported by a FIRC-AIRC fellowship for Italy (i.d. 22318). E.J.M. was supported by a FIRC-AIRC fellowship for Italy (i.d. 25602). The research leading to these results has received funding from AIRC under MFAG 2019 - ID. 22894 project − P.I. Calvaresi Matteo. The paper is published with the contribution of the Department of Excellence program financed by the Minister of Education, University and Research (MIUR, L. 232 del 01/12/2016).

REFERENCES

(1) Perepichka, I. F.; Perepichka, D. F. *Handbook of Thiophene-Based Materials: Applications in Organic Electronics and Photonics*; John Wiley & Sons, Ltd., 2009. DOI: 10.1002/9780470745533.

(2) Barbarella, G.; Zangoli, M.; Di Maria, F. Synthesis and Applications of Thiophene Derivatives as Organic Materials. *Adv. Heterocycl. Chem.* **2017**, *123*, 105−167.

(3) Mazzeo, M.; Mariano, F.; Gigli, G.; Barbarella, G. Organic Light Emitting Diodes Based on Functionalized Oligothiophenes for Display and Lighting Applications. In *Organic Light Emitting Diode*; Sciyo, 2010. DOI: 10.5772/46949.

(4) Zhang, L.; Colella, N. S.; Cherniawski, B. P.; Mannsfeld, S. C. B.; Briseno, A. L. Oligothiophene Semiconductors: Synthesis, Characterization, and Applications for Organic Devices. *ACS Appl. Mater. Interfaces* **2014**, *6* (8), 5327−5343.

(5) Dal Molin, M.; Verolet, Q.; Colom, A.; Letrun, R.; Derivery, E.; Gonzalez-Gaitan, M.; Vauthey, E.; Roux, A.; Sakai, N.; Matile, S. Fluorescent Flippers for Mechanosensitive Membrane Probes. *J. Am. Chem. Soc.* **2015**, *137* (2), 568−571.

(6) Christiansen, D. T.; Tomlinson, A. L.; Reynolds, J. R. New Design Paradigm for Color Control in Anodically Coloring Electrochromic Molecules. *J. Am. Chem. Soc.* **2019**, *141* (9), 3859−3862.

(7) Roncali, J. Molecular Engineering of the Band Gap of π-Conjugated Systems: Facing Technological Applications. *Macromol. Rapid Commun.* **2007**, *28* (17), 1761−1775.

(8) Uhrich, C.; Schueppel, R.; Petrich, A.; Pfeiffer, M.; Leo, K.; Brier, E.; Kilickiran, P.; Baeuerle, P. Organic Thin-Film Photovoltaic Cells Based on Oligothiophenes with Reduced Bandgap. *Adv. Funct. Mater.* **2007**, *17* (15), 2991−2999.

(9) Di Maria, F.; Biasiucci, M.; Di Nicola, F. P.; Fabiano, E.; Zanelli, A.; Gazzano, M.; Salatelli, E.; Lanzi, M.; Della Sala, F.; Gigli, G.; et al. Nanoscale Characterization and Unexpected Photovoltaic Behavior of Low Band Gap Sulfur-Overrich-Thiophene/Benzothiadiazole Decamers and Polymers. *J. Phys. Chem. C* **2015**, *119* (49), 27200−27211.

(10) Kan, B.; Li, M.; Zhang, Q.; Liu, F.; Wan, X.; Wang, Y.; Ni, W.; Long, G.; Yang, X.; Feng, H.; et al. A Series of Simple Oligomer-like Small Molecules Based on Oligothiophenes for Solution-Processed Solar Cells with High Efficiency. *J. Am. Chem. Soc.* **2015**, *137* (11), 3886−3893.

(11) Marinelli, M.; Lanzi, M.; Liscio, A.; Zanelli, A.; Zangoli, M.; Di Maria, F.; Salatelli, E. Single-Material Organic Solar Cells with Fully Conjugated Electron-Donor Alkoxy-Substituted Bithiophene Units and Electron-Acceptor Benzothiadiazole Moieties Alternating in the Main Chain. *J. Mater. Chem. C* **2020**, *8* (12), 4124−4132.

(12) Yue, Q.; Liu, W.; Zhu, X. N-Type Molecular Photovoltaic Materials: Design Strategies and Device Applications. *J. Am. Chem. Soc.* **2020**, *142* (27), 11613−11628.

(13) Hu, H.; Jiang, K.; Yang, G.; Liu, J.; Li, Z.; Lin, H.; Liu, Y.; Zhao, J.; Zhang, J.; Huang, F.; et al. Terthiophene-Based D-A Polymer with an Asymmetric Arrangement of Alkyl Chains That Enables Efficient Polymer Solar Cells. *J. Am. Chem. Soc.* **2015**, *137* (44), 14149−14157.

(14) Peng, R.; Luo, Y.; Cui, Q.; Wang, J.; Li, L. Near-Infrared Conjugated Oligomer for Effective Killing of Bacterial through Combination of Photodynamic and Photothermal Treatment. *ACS Appl. Bio Mater.* **2020**, *3* (2), 1305−1311.

(15) Ma, H.; Liu, C.; Hu, Z.; Yu, P.; Zhu, X.; Ma, R.; Sun, Z.; Zhang, C. H.; Sun, H.; Zhu, S.; et al. Propylenedioxy Thiophene Donor to Achieve NIR-II Molecular Fluorophores with Enhanced Brightness. *Chem. Mater.* **2020**, *32* (5), 2061−2069.

(16) Sun, J.; Li, X.; Du, K.; Feng, F. A Water Soluble Donor-Acceptor-Donor Conjugated Oligomer as a Photosensitizer for Mitochondria-Targeted Photodynamic Therapy. *Chem. Commun.* **2018**, *54* (66), 9194−9197.

(17) Li, J.; Pu, K. Development of Organic Semiconducting Materials for Deep-Tissue Optical Imaging, Phototherapy and Photoactivation. *Chem. Soc. Rev.* **2019**, *48*, 38−71.

(18) Strakova, K.; Lopez-Andarias, J.; Jimenez-Rojo, N.; Chambers, J. E.; Marciniak, S. J.; Riezman, H.; Sakai, N.; Matile, S. Haloflippers: A General Tool for the Fluorescence Imaging of Precisely Localized Membrane Tension Changes in Living Cells. *ACS Cent. Sci.* **2020**, *6* (8), 1376−1385.

(19) Capobianco, M. L.; Barbarella, G.; Manetto, A. Oligothiophenes as Fluorescent Markers for Biological Applications. *Molecules* **2012**, *17* (1), 910−933.

(20) López-Andarias, J.; Straková, K.; Martinent, R.; Jiménez-Rojo, N.; Riezman, H.; Sakai, N.; Matile, S. Genetically Encoded Supramolecular Targeting of Fluorescent Membrane Tension Probes within Live Cells: Precisely Localized Controlled Release by External Chemical Stimulation. *JACS Au* **2021**, *1*, 221−232.

(21) Di Maria, F.; Palamà, I. E.; Baroncini, M.; Barbieri, A.; Bongini, A.; Bizzarri, R.; Gigli, G.; Barbarella, G. Live Cell Cytoplasm Staining and Selective Labeling of Intracellular Proteins by Non-Toxic Cell-Permeant Thiophene Fluorophores. *Org. Biomol. Chem.* **2014**, *12* (10), 1603−1610.

(22) Cieślar-Pobuda, A.; Bäck, M.; Magnusson, K.; Jain, M. V.; Rafat, M.; Ghavami, S.; Nilsson, K. P. R.; Los, M. J. Cell Type Related Differences in Staining with Pentameric Thiophene Derivatives. *Cytometry, Part A* **2014**, *85* (7), 628−635.

(23) Zambianchi, M.; Di Maria, F.; Cazzato, A.; Gigli, G.; Piacenza, M.; Della Sala, F.; Barbarella, G. Microwave-Assisted Synthesis of Thiophene Fluorophores, Labeling and Multilabeling of Monoclonal Antibodies, and Long Lasting Staining of Fixed Cells. *J. Am. Chem. Soc.* **2009**, *131* (31), 10892−10900.

(24) Calvo-Rodriguez, M.; Hou, S. S.; Snyder, A. C.; Dujardin, S.; Shirani, H.; Nilsson, K. P. R.; Bacskai, B. J. In Vivo Detection of Tau Fibrils and Amyloid β Aggregates with Luminescent Conjugated Oligothiophenes and Multiphoton Microscopy. *Acta Neuropathol. Commun.* **2019**, *7* (1), 171.

(25) Åslund, A.; Sigurdson, C. J.; Klingstedt, T.; Grathwohl, S.; Bolmont, T.; Dickstein, D. L.; Glimsdal, E.; Prokop, S.; Lindgren, M.; Konradsson, P.; et al. Novel Pentameric Thiophene Derivatives for in Vitro and in Vivo Optical Imaging of a Plethora of Protein Aggregates in Cerebral Amyloidoses. *ACS Chem. Biol.* **2009**, *4* (8), 673−684.

(26) Moros, M.; Di Maria, F.; Dardano, P.; Tommasini, G.; Castillo-Michel, H.; Kovtun, A.; Zangoli, M.; Blasio, M.; De Stefano, L.; Tino, A.; et al. In Vivo Bioengineering of Fluorescent Conductive Protein-Dye Microfibers. *iScience* **2020**, *23* (4), 101022.

(27) Herland, A.; Nilsson, K. P. R.; Olsson, J. D. M.; Hammarström, P.; Konradsson, P.; Inganäs, O. Synthesis of a Regioregular Zwitterionic Conjugated Oligoelectrolyte, Usable as an Optical Probe for Detection of Amyloid Fibril Formation at Acidic PH. *J. Am. Chem. Soc.* **2005**, *127* (7), 2317−2323.

(28) He, Z.; Zhao, L.; Zhang, Q.; Chang, M.; Li, C.; Zhang, H.; Lu, Y.; Chen, Y. An Acceptor-Donor-Acceptor Structured Small Molecule for Effective NIR Triggered Dual Phototherapy of Cancer. *Adv. Funct. Mater.* **2020**, *30* (16), 1910301.

(29) Fuse, S.; Takizawa, M.; Matsumura, K.; Sato, S.; Okazaki, S.; Nakamura, H. Thiophene-Based Organic D-π-A Dyes as Potent Sensitizers for Photodynamic Therapy. *Eur. J. Org. Chem.* **2017**, *2017* (34), 5170−5177.

(30) Zangoli, M.; Di Maria, F. Synthesis, Characterization, and Biological Applications of Semiconducting Polythiophene-based Nanoparticles. *View* **2021**, *2* (1), 20200086.

(31) Zhou, H.; Zeng, X.; Li, A.; Zhou, W.; Tang, L.; Hu, W.; Fan, Q.; Meng, X.; Deng, H.; Duan, L.; et al. Upconversion NIR-II Fluorophores for Mitochondria-Targeted Cancer Imaging and Photothermal Therapy. *Nat. Commun.* **2020**, *11* (1), 6183.

(32) Jung, H. S.; Verwilst, P.; Sharma, A.; Shin, J.; Sessler, J. L.; Kim, J. S. Organic Molecule-Based Photothermal Agents: An Expanding Photothermal Therapy Universe. *Chem. Soc. Rev.* **2018**, *47*, 2280−2297.

(33) Wang, S.; Chen, H.; Liu, J.; Chen, C.; Liu, B. NIR-II Light Activated Photosensitizer with Aggregation-Induced Emission for Precise and Efficient Two-Photon Photodynamic Cancer Cell Ablation. *Adv. Funct. Mater.* **2020**, *30* (30), 2002546.

(34) Dolmans, D. E. J. G. J.; Fukumura, D.; Jain, R. K. Photodynamic Therapy for Cancer. *Nat. Rev. Cancer* **2003**, *3*, 380−387.

https://doi.org/10.1021/jacsau.1c00061
JACS Au 2021, 1, 925−935

(35) Shi, H.; Sadler, P. J. How Promising Is Phototherapy for Cancer? *Br. J. Cancer* **2020**, *123*, 871−873.
(36) Weinberg, F.; Ramnath, N.; Nagrath, D. Reactive Oxygen Species in the Tumor Microenvironment: An Overview. *Cancers* **2019**, *11* (8), 1191.
(37) Aggarwal, V.; Tuli, H. S.; Varol, A.; Thakral, F.; Yerer, M. B.; Sak, K.; Varol, M.; Jain, A.; Khan, M. A.; Sethi, G. Role of Reactive Oxygen Species in Cancer Progression: Molecular Mechanisms and Recent Advancements. *Biomolecules* **2019**, *9* (11), 735.
(38) Jia, P.; Dai, C.; Cao, P.; Sun, D.; Ouyang, R.; Miao, Y. The Role of Reactive Oxygen Species in Tumor Treatment. *RSC Adv.* **2020**, *10*, 7740−7750.
(39) Celli, J. P.; Spring, B. Q.; Rizvi, I.; Evans, C. L.; Samkoe, K. S.; Verma, S.; Pogue, B. W.; Hasan, T. Imaging and Photodynamic Therapy: Mechanisms, Monitoring, and Optimization. *Chem. Rev.* **2010**, *110* (5), 2795−2838.
(40) Barth, C. W.; Gibbs, S. Fluorescence Image-Guided Surgery: A Perspective on Contrast Agent Development; *Proc. SPIE Int. Soc. Opt. Eng.* **2020**, *11222*, 112220J.
(41) Di Giosia, M.; Solda, A.; Seeger, M.; Cantelli, A.; Arnesano, F.; Nardella, M. I.; Mangini, V.; Valle, F.; Montalti, M.; Zerbetto, F.; Rapino, S.; Calvaresi, M.; Ntziachristos, V. A Bio-Conjugated Fullerene as a Subcellular-Targeted and Multifaceted Phototheranostic Agent. *Adv. Funct. Mater.* **2021**, 2101527.
(42) Simões, J. C. S.; Sarpaki, S.; Papadimitroulas, P.; Therrien, B.; Loudos, G. Conjugated Photosensitizers for Imaging and PDT in Cancer Research. *J. Med. Chem.* **2020**, *63* (23), 14119−14150.
(43) Abrahamse, H.; Hamblin, M. R. New Photosensitizers for Photodynamic Therapy. *Biochem. J.* **2016**, *473* (4), 347−364.
(44) Lan, M.; Zhao, S.; Liu, W.; Lee, C. S.; Zhang, W.; Wang, P. Photosensitizers for Photodynamic Therapy. *Adv. Healthcare Mater.* **2019**, *8* (13), No. e1900132.
(45) Middha, E.; Liu, B. Nanoparticles of Organic Electronic Materials for Biomedical Applications. *ACS Nano* **2020**, *14* (8), 9228−9242.
(46) Wan, Y.; Lu, G.; Wei, W. C.; Huang, Y. H.; Li, S.; Chen, J. X.; Cui, X.; Xiao, Y. F.; Li, X.; Liu, Y.; et al. Stable Organic Photosensitizer Nanoparticles with Absorption Peak beyond 800 Nanometers and High Reactive Oxygen Species Yield for Multimodality Phototheranostics. *ACS Nano* **2020**, *14* (8), 9917−9928.
(47) Maya-Vetencourt, J. F.; Manfredi, G.; Mete, M.; Colombo, E.; Bramini, M.; Di Marco, S.; Shmal, D.; Mantero, G.; Dipalo, M.; Rocchi, A.; et al. Subretinally Injected Semiconducting Polymer Nanoparticles Rescue Vision in a Rat Model of Retinal Dystrophy. *Nat. Nanotechnol.* **2020**, *15* (8), 698−708.
(48) Bargigia, I.; Zucchetti, E.; Kandada, A. R. S.; Moreira, M.; Bossio, C.; Wong, W. P. D.; Miranda, P. B.; Decuzzi, P.; Soci, C.; D'Andrea, C.; et al. The Photophysics of Polythiophene Nanoparticles for Biological Applications. *ChemBioChem* **2019**, *20* (4), 532−536.
(49) Fuse, S.; Takizawa, M.; Sato, S.; Okazaki, S.; Nakamura, H. Elucidating the Mode of Action for Thiophene-Based Organic D-π-A Sensitizers for Use in Photodynamic Therapy. *Bioorg. Med. Chem.* **2019**, *27* (2), 315−321.
(50) Konan, Y. N.; Gurny, R.; Allémann, E. State of the Art in the Delivery of Photosensitizers for Photodynamic Therapy. *J. Photochem. Photobiol., B* **2002**, *66* (2), 89−106.
(51) Debele, T. A.; Peng, S.; Tsai, H.-C. Drug Carrier for Photodynamic Cancer Therapy. *Int. J. Mol. Sci.* **2015**, *16* (9), 22094−22136.
(52) Soldà, A.; Cantelli, A.; Di Giosia, M.; Montalti, M.; Zerbetto, F.; Rapino, S.; Calvaresi, M. C60@lysozyme: A New Photosensitizing Agent for Photodynamic Therapy. *J. Mater. Chem. B* **2017**, *5* (32), 6608−6615.
(53) Di Giosia, M.; Bomans, P. H. H.; Bottoni, A.; Cantelli, A.; Falini, G.; Franchi, P.; Guarracino, G.; Friedrich, H.; Lucarini, M.; Paolucci, F.; et al. Proteins as Supramolecular Hosts for C60: A True Solution of C60 in Water. *Nanoscale* **2018**, *10* (21), 9908−9916.
(54) Di Giosia, M.; Nicolini, F.; Ferrazzano, L.; Soldà, A.; Valle, F.; Cantelli, A.; Marforio, T. D.; Bottoni, A.; Zerbetto, F.; Montalti, M.; et al. Stable and Biocompatible Monodispersion of C 60 in Water by Peptides. *Bioconjugate Chem.* **2019**, *30* (3), 808−814.
(55) Cantelli, A.; Piro, F.; Pecchini, P.; Di Giosia, M.; Danielli, A.; Calvaresi, M. Concanavalin A-Rose Bengal Bioconjugate for Targeted Gram-Negative Antimicrobial Photodynamic Therapy. *J. Photochem. Photobiol., B* **2020**, *206*, 111852.
(56) Abbas, M.; Zou, Q.; Li, S.; Yan, X. Self-Assembled Peptide- and Protein-Based Nanomaterials for Antitumor Photodynamic and Photothermal Therapy. *Adv. Mater.* **2017**, *29* (12), 1605021.
(57) Callmann, C. E.; Leguyader, C. L. M.; Burton, S. T.; Thompson, M. P.; Hennis, R.; Barback, C.; Henriksen, N. M.; Chan, W. C.; Jaremko, M. J.; Yang, J.; et al. Antitumor Activity of 1,18-Octadecanedioic Acid-Paclitaxel Complexed with Human Serum Albumin. *J. Am. Chem. Soc.* **2019**, *141* (30), 11765−11769.
(58) Yu, C.; Huang, F.; Chow, W. A.; Cook-Wiens, G.; Cui, X. Single Protein Encapsulated Doxorubicin as an Efficacious Anticancer Therapeutic. *Adv. Ther.* **2020**, *3* (11), 2000135.
(59) Zhang, P.; Huang, H.; Banerjee, S.; Clarkson, G. J.; Ge, C.; Imberti, C.; Sadler, P. J. Nucleus-Targeted Organoiridium-Albumin Conjugate for Photodynamic Cancer Therapy. *Angew. Chem., Int. Ed.* **2019**, *58* (8), 2350−2354.
(60) Rong, P.; Huang, P.; Liu, Z.; Lin, J.; Jin, A.; Ma, Y.; Niu, G.; Yu, L.; Zeng, W.; Wang, W.; et al. Protein-Based Photothermal Theranostics for Imaging-Guided Cancer Therapy. *Nanoscale* **2015**, *7* (39), 16330−16336.
(61) Chen, Q.; Wang, C.; Zhan, Z.; He, W.; Cheng, Z.; Li, Y.; Liu, Z. Near-Infrared Dye Bound Albumin with Separated Imaging and Therapy Wavelength Channels for Imaging-Guided Photothermal Therapy. *Biomaterials* **2014**, *35* (28), 8206−8214.
(62) Hoogenboezem, E. N.; Duvall, C. L. Harnessing Albumin as a Carrier for Cancer Therapies. *Adv. Drug Delivery Rev.* **2018**, *130*, 73−89.
(63) Chen, Q.; Liu, Z. Albumin Carriers for Cancer Theranostics: A Conventional Platform with New Promise. *Adv. Mater.* **2016**, *28* (47), 10557−10566.
(64) Chao, C. Y.; Chao, C. H.; Chen, L. P.; Hung, Y. C.; Lin, S. T.; Su, W. F.; Lin, C. F. Band Structure Engineering for Low Band Gap Polymers Containing Thienopyrazine. *J. Mater. Chem.* **2012**, *22* (15), 7331−7341.
(65) Hwang, Y. J.; Kim, F. S.; Xin, H.; Jenekhe, S. A. New Thienothiadiazole-Based Conjugated Copolymers for Electronics and Optoelectronics. *Macromolecules* **2012**, *45* (9), 3732−3739.
(66) Canola, S.; Mardegan, L.; Bergamini, G.; Villa, M.; Acocella, A.; Zangoli, M.; Ravotto, L.; Vinogradov, S. A.; Di Maria, F.; Ceroni, P.; et al. One- and Two-Photon Absorption Properties of Quadrupolar Thiophene-Based Dyes with Acceptors of Varying Strengths. *Photochem. Photobiol. Sci.* **2019**, *18* (9), 2180−2190.
(67) Redmond, R. W.; Gamlin, J. N. A Compilation of Singlet Oxygen Yields from Biologically Relevant Molecules. *Photochem. Photobiol.* **1999**, *70* (4), 391−475.
(68) Liu, Q.; Guan, M.; Xu, L.; Shu, C.; Jin, C.; Zheng, J.; Fang, X.; Yang, Y.; Wang, C. Structural Effect and Mechanism of C_{70}-Carboxyfullerenes as Efficient Sensitizers against Cancer Cells. *Small* **2012**, *8* (13), 2070−2077.
(69) Zhang, T.; Li, Y.; Zheng, Z.; Ye, R.; Zhang, Y.; Kwok, R. T. K.; Lam, J. W. Y.; Tang, B. Z. In Situ Monitoring Apoptosis Process by a Self-Reporting Photosensitizer. *J. Am. Chem. Soc.* **2019**, *141* (14), 5612−5616.
(70) Plaetzer, K.; Kiesslich, T.; Oberdanner, C.; Krammer, B. Apoptosis Following Photodynamic Tumor Therapy: Induction, Mechanisms and Detection. *Curr. Pharm. Des.* **2005**, *11* (9), 1151−1165.
(71) Sun, H.; Lv, F.; Liu, L.; Gu, Q.; Wang, S. Conjugated Polymer Materials for Photothermal Therapy. *Adv. Ther.* **2018**, *1* (6), 1800057.
(72) Sun, T.; Dou, J. H.; Liu, S.; Wang, X.; Zheng, X.; Wang, Y.; Pei, J.; Xie, Z. Second Near-Infrared Conjugated Polymer Nanoparticles for Photoacoustic Imaging and Photothermal Therapy. *ACS Appl. Mater. Interfaces* **2018**, *10* (9), 7919−7926.

https://doi.org/10.1021/jacsau.1c00061
JACS Au 2021, 1, 925−935

(73) Bolze, F.; Jenni, S.; Sour, A.; Heitz, V. Molecular Photosensitisers for Two-Photon Photodynamic Therapy. *Chem. Commun.* **2017**, *53* (96), 12857−12877.
(74) Cieplik, F.; Deng, D.; Crielaard, W.; Buchalla, W.; Hellwig, E.; Al-Ahmad, A.; Maisch, T. Antimicrobial Photodynamic Therapy-What We Know and What We Don't. *Crit. Rev. Microbiol.* **2018**, *44* (5), 571−589.
(75) Schindelin, J.; Arganda-Carreras, I.; Frise, E.; Kaynig, V.; Longair, M.; Pietzsch, T.; Preibisch, S.; Rueden, C.; Saalfeld, S.; Schmid, B.; et al. Fiji: An Open-Source Platform for Biological-Image Analysis. *Nat. Methods* **2012**, *9*, 676−682.

https://doi.org/10.1021/jacsau.1c00061
JACS Au 2021, 1, 925−935